Modeling the energy and momentum dependent loss function of the valence shells of liquid water

D. Emfietzoglou [a,c,*], A. Pathak [b,1], M. Moscovitch [c]

[a] *Department of Medical Physics, University of Ioannina Medical School, Ioannina 451 10, Greece*
[b] *School of Physics, University of Hyderabad, Hyderabad 500 046, India*
[c] *Department of Radiation Medicine, Georgetown University Medical Center, Washington, DC 20007, USA*

Abstract

Within the Born approximation the loss function is the important material property for describing the inelastic interaction of charged particles with the extended electronic subsystem of condensed media. Following the dielectric approach as elaborated by Ritchie and co-workers we determine the loss function of liquid water by a two-step process: (i) an optical energy-loss model is deduced by an analytic representation of the available data at the long wavelength limit, and (ii) the momentum dependence is introduced by simple dispersion models which provide characteristic features of the Bethe surface. By this semi-empirical procedure many-body effects such as polarization, correlation and collective excitations, which are still impractical to compute, are accounted for in a self-consistent manner. Effects on the Bethe surface characteristics of liquid water associated with the choice of the optical-data model and its extension to the momentum plane are explored.
© 2004 Elsevier B.V. All rights reserved.

Keywords: Inelastic interaction; Dielectric function; Water

1. Introduction

The inelastic interaction of charged particles with the extended electronic subsystem of con-

densed media is best described by the dielectric function properties of the medium, as first shown by Lindhard, Hubbard and Ritchie in the 1950s. The dielectric formalism was subsequently applied by Fano to various penetration phenomena in solids extending Bethe's stopping theory [1]. At the heart of this formalism is the generalization of the dielectric constant of a medium, ε, to a complex dielectric function, $\varepsilon(\omega, K) = \varepsilon_1(\omega, K) + i\varepsilon_2(\omega, K)$, where $E = \hbar\omega$ and $q = \hbar K$ are the energy- and momentum-transfer, respectively (we

* Corresponding author. Address: Department of Medical Physics, University of Ioannina Medical School, Ioannina 451 10, Greece. Tel.: +30 26510 97741; fax: +30 26510 97854.
E-mail address: demfietz@cc.uoi.gr (D. Emfietzoglou).
[1] Sabbatical address till January 2005: Departmento de Fisica, UAM Iztapalapa, Mexico.

refer to the isotropic and homogeneous case where K is scalar). This generalization accounts for the absorption (E-dependence) and scattering (q-dependence) properties of the medium to external perturbations. In particular, the imaginary part of the inverse dielectric function:

$$\text{Im}\left[\frac{-1}{\varepsilon(E,q)}\right] = \frac{\varepsilon_2(E,q)}{\varepsilon_1^2(E,q) + \varepsilon_2^2(E,q)} = \frac{\text{Im}[\varepsilon(E,q)]}{|\varepsilon(E,q)|^2}$$
(1)

plays a central role in the slowing-down process and is called the energy-loss function or simply the loss function (LF) of the material. Its three-dimensional representation in the E–q plane defines the material's Bethe surface. In fact, whereas the numerator in Eq. (1) corresponds to the standard single-particle transitions of an atom or molecule in the gas phase, the denominator accounts for the influence of the condensed phase. That is, the polarization of the medium by the charged particle field is represented by a screening ($|\varepsilon| > 1$) or a collective anti-screening effect ($|\varepsilon| < 1$), whereas at high enough frequencies the limit $|\varepsilon| \approx 1$, typical of the gas phase, is approached. Within the first Born approximation, the LF directly determines the doubly-differential cross-section of non-relativistic particles:

$$\frac{d^2\lambda^{-1}(T,E,q)}{dE\,dq} = \frac{1}{\pi\alpha_0 Tq}\text{Im}\left[\frac{-1}{\varepsilon(E,q)}\right],$$
(2)

where λ^{-1} is the inelastic inverse mean-free-path, α_0 the Bohr radius, and $T = mv^2/2$ with m the electron rest mass and v the particle velocity. Various integrals of the LF are also associated with important transport parameters by means of

$$M^{(n)}(T) = \frac{1}{\pi\alpha_0 T}\int E^n\,dE\int \frac{1}{q}\text{Im}\left[\frac{-1}{\varepsilon(E,q)}\right]dq,$$
(3)

where for $n = 0, 1, 2$, the inelastic mean-free-path, the electronic stopping-power and the straggling parameter, respectively, are obtained.

Therefore, efforts have been made to develop accurate and computationally tractable algorithms for the evaluation of the LF to be used for realistic Monte Carlo simulation of particle transport in condensed matter [2], as well as for a first-principle calculation of electronic stopping-powers below

Bethe's cut-off [3]. In the present work, we provide (i) an analytic parametrization of the recent Inelastic X-ray Scattering Spectroscopy (IXSS) data at $q = 0$ [4] for liquid water by means of our previously developed optical-data model (ODM), and (ii) a detailed evaluation of the energy-momentum variation of LF of liquid water, by use of our ODM and several dispersion algorithms, and a comparison of the model LF against the IXXS data in the range $0.69 \leqslant q \leqslant 3.59$ a.u. [5].

2. Methodology

2.1. The dielectric function formalism

In principle, the LF may be obtained on the basis of the microscopic system's Hamiltonian since it is directly associated to the electronic degrees of freedom. Thus, formally, the LF is proportional to the dynamic-structure-factor (or the inelastic form-factor), $S(q, E)$, by means of

$$\text{Im}\left[\frac{-1}{\varepsilon(E,q)}\right] = \frac{\pi}{2Z}\frac{E_p^2}{R(K\alpha_0)^2}S(E,q),$$
(4a)

$$S(E,q) = \sum_f \left|\left\langle f\left|\sum_{j=1}^Z \exp(iKr_j)\right|i\right\rangle\right|^2,$$
(4b)

where E_p is the (nominal) plasma energy, Z is the number of electrons with r_j the coordinates of the jth electron and $|i\rangle$, $|f\rangle$ are the initial and final state wave-functions, respectively. Calculations by means of Eqs. (4a) and (4b), however, are still impractical for condensed media due to the strong many-body character. Although significant advances have been made for ground-state calculations, excited electronic states, which are of interest here, still present a daunting task [6]. On the other hand, the LF may also be obtained by macroscopic methods, e.g. by various spectroscopic techniques (EELS, IXSS), whereas its long wavelength limit may be obtained by optical measurements. This association of the LF with observable quantities has been a key factor for the widespread application of the dielectric formalism, as elaborated by the Oak Ridge group (Ritchie,

Ashley and co-workers) [7]. Their methodology is particularly suitable for non-free-electron-like materials, such as liquid water. It is a two-step process where one starts with an analytic representation of the experimental data at the optical limit and then introduces the momentum dependence by a simple dispersion algorithm. This is an economic, yet consistent method for obtaining the LF with only a minimum of computational effort. Moreover, the only input required are optical data which are available for many materials, whereas its experimental origin accounts, by default, for many-body effects such as polarization, correlation and collective excitations, which are still impractical to compute.

2.2. Optical-data models

An optical-data model (ODM) refers to an analytic representation of the experimental data at long wavelengths ($K \ll 1$) of the imaginary part of either ε or $-1/\varepsilon$. An ODM provides, therefore, the dependence of the inelastic probability on energy loss at the optical limit ($q = 0$) (see Eq. (2)) and, as a corollary, a model of the optical region of the Bethe surface. The 30-year old optical measurements at Oak-Ridge [8] have provided the basis for all studies conducted so far for liquid water [9, and references therein]. Based on these data we have previously constructed an ODM using a linear superposition of modified-Drude functions, which improved earlier models [10]. An important shortcoming of these data, however, was the limited energy range covered (up to 25 eV) which was not sufficient to exhaust the influence of condensation (i.e. $|\varepsilon| \neq 1$). Also, the somewhat conspicuously large peak at about the plasmon energy of liquid water (21–22 eV) had raised concerns on the existence of a strong collective excitation [11]. The new IXSS data [4,5] (i) extend to much higher energies ($\sim$200 eV), and (ii) provide, for the first time, evidence for the q-dependence of the LF. The analytic parametrization of the new data followed the previous methodology [10] where the Drude-model constants for the various single-electron transitions were used as adjustable parameters.

2.3. Dispersion models

A dispersion model provides a scheme for incorporating the q-dependence on Im$(-1/\varepsilon)$ and, thus, guides the construction of the Bethe surface along the momentum plane. The latter is still unknown for realistic materials and, consequently, no definite method exists for modeling the q-dependence. This state of affair has led to various heuristic approaches, which are basically meant to account for the most important features of the Bethe surface, such as, for example, the development of the Bethe ridge. For free-electron-like materials, Lindhard's or (Mermin's) dielectric function provides the basis for the q-dependence [12]. Their suitability, however, for the single-electron valence-shell transitions of liquid water (and other organic materials) is questionable [13]. In previous studies we have implemented various dispersion models to our ODM, such as, the δ-oscillator schemes of Ashley and Liljequist, and Ritchie's extended-Drude schemes, and calculated electron [3,10] and proton [14] inelastic characteristics for liquid water. A brief description of the resultant model LFs follows.

2.3.1. δ-oscillator models

Following [12], the optical-oscillator-strength density of an atom may be represented by the following relationship:

$$\frac{\mathrm{d}f(E,0)}{\mathrm{d}E} = \sum_j f_j \delta(E - E_j), \tag{5}$$

where j denotes a particular transition. The δ-function in Eq. (5) may be called an optical-oscillator. This idea may be used to extend the optical function to $q > 0$ by substituting E_j with a dispersion function $G_j(q)$ such as $G_j(0) = E_j$. By using the relationship between the oscillator-strength and the loss function,

$$\frac{\mathrm{d}f(E,q)}{\mathrm{d}E} = \frac{2Z}{\pi} \frac{E}{E_p^2} \mathrm{Im}\left[\frac{-1}{\varepsilon(E,q)}\right], \tag{6}$$

Eq. (5) may be appropriately generalized to

$$E\,\mathrm{Im}\left[\frac{-1}{\varepsilon(E,q)}\right] = \int_0^\infty E'\mathrm{Im}\left[\frac{-1}{\varepsilon(E',0)}\right]\delta(E - G(E';q))\,\mathrm{d}E'. \tag{7}$$

The δ-function may now be called the δ-oscillator. Ashley [15] has provided the following dispersion to be used in the δ-oscillator of Eq. (7):

$$G(E'; q) = E' + q^2/2m. \tag{8}$$

It resembles the plasmon dispersion of the free-electron gas at low-q, while asymptotically leading to the Bethe ridge at high-q. By inserting Eq. (8) into Eq. (7), the following LF formula is obtained:

$$\mathrm{Im}\left[\frac{-1}{\varepsilon(E,q)}\right] = \int_0^\infty E'\mathrm{Im}\left[\frac{-1}{\varepsilon(E',0)}\right]\frac{\delta(E-(E'+q^2/2m))}{E}\,\mathrm{d}E'. \tag{9}$$

Eq. (9) essentially amounts to a quadratic extension into the E–q plane.

Liljequist [16] has suggested a dispersion scheme based on Bohr's distinction between resonant-like and binary-like collisions. The former correspond to the optical region of the Bethe surface, whereas the latter define the Bethe ridge. The following dispersion scheme was suggested:

$$\begin{aligned} G(E'; q) &= E' \quad \text{for } q^2/2m \leqslant E', \\ G(E'; q) &= q^2/2m \quad \text{for } q^2/2m > E'. \end{aligned} \tag{10}$$

By inserting Eq. (10) in Eq. (7) the following LF formula is obtained:

$$\begin{aligned} &\mathrm{Im}\left[\frac{-1}{\varepsilon(E,q)}\right] \\ &= \int_0^\infty E'\mathrm{Im}\left[\frac{-1}{\varepsilon(E',0)}\right]\frac{\delta(E-E')}{E}\Theta(E'-q^2/2m)\,\mathrm{d}E' \\ &\quad + \int_0^\infty E'\mathrm{Im}\left[\frac{-1}{\varepsilon(E',0)}\right]\frac{\delta(E-q^2/2m)}{E}\Theta(q^2/2m-E')\,\mathrm{d}E'. \end{aligned} \tag{11}$$

Eq. (11) may be simplified to

$$\begin{aligned} \mathrm{Im}\left[\frac{-1}{\varepsilon(E,q)}\right] &= \mathrm{Im}\left[\frac{-1}{\varepsilon(E,0)}\right]\Theta(E-q^2/2m) \\ &\quad + E_p^2\frac{\pi}{2}\frac{Z_{\mathrm{eff}}(q)}{Z}\frac{\delta(E-q^2/2m)}{E}, \end{aligned} \tag{12}$$

where $Z_{\mathrm{eff}}(q)$ is the effective number of target electrons which participate in collisions with energy transfer up to $q^2/2m$, as obtained from the relevant sum-rule. Note that in Eq. (12) the extension to the momentum plane is practically obtained by simply extending part of the optical loss function to finite momentum values ($E > q^2/2m$ region) and by

placing delta functions along the Bethe ridge; the latter corresponds to the $E < q^2/2m$ region.

2.3.2. Extended-Drude schemes

Given a Drude-type representation of the optical spectrum, Ritchie [17] has suggested that the q-dependence may be incorporated in the (empirical) model parameters by a substitution of the type $\{f_j, \gamma_j, E_j\} \rightarrow \{f_j(q), \gamma_j(q), E_j(q)\}$; the simplest one is the use of the triad $\{f_j, \gamma_j, E_j(q)\}$, where $E_j(q)$ is given by the impulse-approximation:

$$E_j(q) = E_j(0) + q^2/2m. \tag{13}$$

To avoid the unrealistic free-electron-like dispersion of the discrete transitions one may restrict Eq. (13) to the continuum i.e. $E_j(q) \rightarrow E_{j,\mathrm{cont.}}(q)$, and subsequently adopt an empirically-derived GOS for the free-molecule, i.e. the use of the triad $\{f_j(q), \gamma_j, E_j(q)\}$. An analytic function of the general form:

$$f_{\mathrm{exc}}^{(j)}(q) = f_{\mathrm{exc}}^{(j)}(0)\sum_n a_n^{(j)}q^n \exp(-b_n^{(j)}q) \tag{14}$$

has been adopted by Ritchie and co-workers [7] for the discrete transitions. By means of the f-sum rule the corresponding q-dependence of the continuum may be obtained:

$$f_{\mathrm{ioniz}}^{(j)}(q) = f_{\mathrm{ioniz}}^{(j)}(0)\frac{1 - \sum_j f_{\mathrm{exc}}^{(j)}(q)}{1 - \sum_j f_{\mathrm{exc}}^{(j)}(0)}. \tag{15}$$

Although the generalised-oscillator-strength of the liquid will, obviously, bear a q-dependence that will be different from the one of the free molecule, the above approximation provides a more reasonable q-dependence for the discrete than the one provided by Eq. (13). Moreover, phase differences are expected to be more important at $q = 0$ (where the liquid absorption spectrum has been used), gradually vanishing at large q.

3. Results and discussion

In Figs. 1(a) and (b) we compare the dielectric functions as obtained by our ODMs against the two sets of experimental data in the region from threshold to 50 eV where condensed phase effects

are most pronounced. Although not shown, the ODMs account for all individual single-electron valence transitions of water (eight discrete excitations and four ionization shells). The parametrization of the new ODM may be provided by the authors upon request. The representation of both sets of data is very good, especially with respect to the optical loss function, $Im[-1/\varepsilon(E, 0)]$, which is the key material property. Although not shown, this agreement extends up to the highest experimental data point (~200 eV for the IXSS data). Interestingly, a comparison between the two ODMs at the 21 eV region reveals that the new $Im[-1/\varepsilon(E, 0)]$ is by a factor of 1.5 lower, whereas

the new $Re[\varepsilon]$ is by a factor of 2 higher. Thus, the new optical data further support the hypothesis that the 21 eV peak, though of some collective character, is not due to a plasmon excitation. The ODMs satisfy the sum-rules to within 0.5–1.5%, whereas an I-value between 80 and 85 eV is obtained depending on the ODM used. The I-values are slightly higher than the ICRUI-value for liquid water (75 ± 3 eV) [18], but in better agreement with more recent experiments (79.7 ± 0.5 eV) [19] and calculations (81.8 eV) [20].

The influence of the ODM on the dispersion characteristics is examined in Figs. 2(a) and (b). The LFs predicted by the two ODMs (using the extended-Drude dispersion in both) are compared as a function of the energy transfer (Fig. 2(a)) and momentum transfer (Fig. 2(b)) for several values of q and E, respectively. The new ODM predicts (i) an energy loss spectrum skewed towards higher losses, which further supports the idea of strong inter-molecular perturbation effects in the liquid phase by contrast to the vapor (this effect gradually vanishes though at $q > 0$), and (ii) a much broader momentum distribution, which is indicative of stronger intra-molecular binding effects.

The three-dimensional profile of the LF in the $E–q$ plane, i.e. the Bethe surface of the material, is examined in the subsequent figures. In Fig. 3(a) the Bethe surface of liquid water as determined by the IXSS data which cover the range $0.69 \leqslant q \leqslant 3.59$ a.u. [5] is shown. Model calculations of the Bethe surface of liquid water are depicted in Figs. 3(b) and (c). In particular, in Fig. 3(b) we have calculated the energy–momentum variation of the loss function by means of the ODM established from the reflectance data of [8] and the extended-Drude model. The calculations of Fig. 3(c), on the other hand, make use of the ODM established from the IXSS data of [4]; while the dispersion is the same as in Fig. 3(b). The Bethe surface model of Fig. 3(b) has been adopted in our MC code for charged particle transport calculations in liquid water [9] and has also been used, with some variation, in the OREC (Oak Ridge) [21] and PARTRAC (GSF) [22] MC codes. In agreement with an earlier study [23], the semi-empirical Bethe surface based on ODMs and the extended-Drude dispersion is in fair agreement
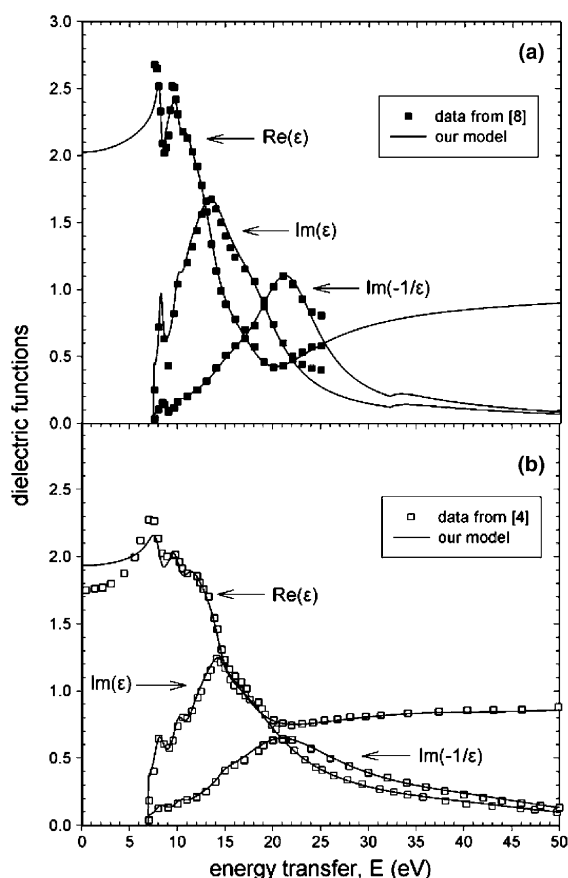
Fig. 1. The dielectric response functions of liquid water at the optical limit – full-curves: our optical-data models; boxes: (a) reflectance data [8], (b) IXSS data [4].
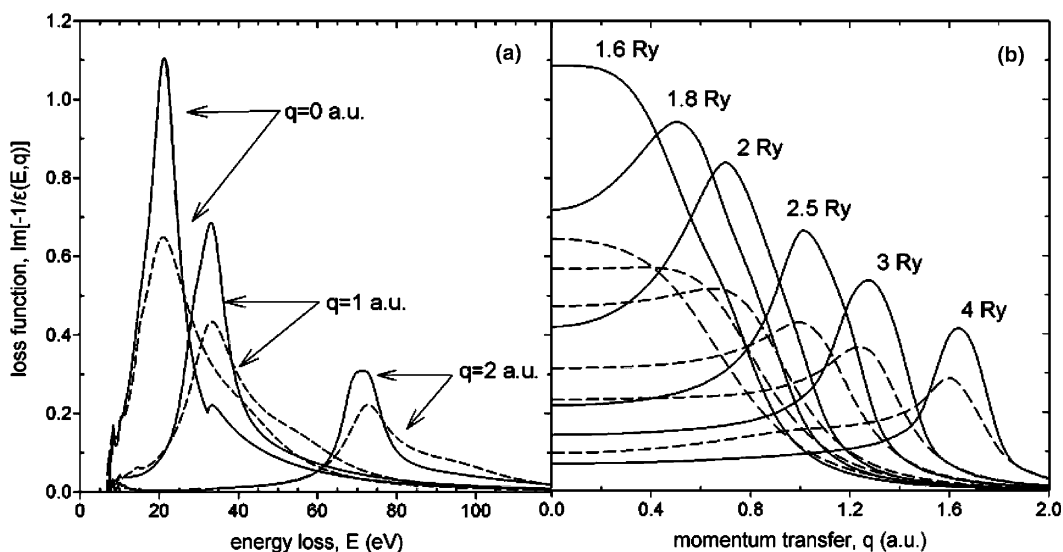
Fig. 2. The loss function of liquid water as a function of (a) the energy transfer and (b) the momentum transfer. Full-line: based on the optical-data model established from the reflectance data of [8]; broken-line: based on the optical-data model established from the IXSS data of [4]. The extended-Drude dispersion model is used for both calculations.

with the experimental Bethe surface as far as the global characteristics are concerned. This provides some confidence on the overall reliability of the approximations used in the model dielectric functions. Although not shown, the Bethe surface obtained by the plasmon-like δ-oscillator model exhibits very similar characteristics; especially with respect to the development of the Bethe ridge. In contrast, the δ-oscillator model using the simplified resonant-binary distinction provides the crudest approximation of the Bethe surface with practically most of its loss function concentrated along a delta-like Bethe ridge.

Further insight upon the above issue is provided in Figs. 4(a) and (b), where the difference between the model LF and the experimental LF is depicted as a surface in the energy–momentum plane. The model calculation in panel (a) is as in Fig. 3(b), whereas, in panel (b) as in Fig. 3(c). Despite the fact that the experimental Bethe surface, as shown in Fig. 3(a), appears to also evolve in a quadratic-like mode, it is much broader in shape than the model calculations since there is a pronounced positive surface difference all along the Bethe ridge in both Figs. 4(a) and (b). That is, the free-electron limit is approached much faster

by the dispersion model which underestimates binding effects at finite momentum values. By comparing the two panels of Fig. 4 it is apparent that the choice of the ODM adopted has an important effect even in the region of finite momentum; in particular, the use of the reflectance data of [8], which form the basis for all dielectric calculations made so far for liquid water, leads to substantially higher surface difference throughout the entire energy–momentum plane.

The heuristic, though physically plausible, nature of the various dispersion models and the lack of any experimental verification had always been the main point of criticism in the application of the dielectric methodology to liquid water (and other non-free-electron-like materials). In the light of the recent data on the near complete optical spectrum of the valence shells of liquid water, as well as on the momentum dependence of its dielectric functions, the present study showed that, despite their internal consistency, the dielectric models used so far for liquid water may need some refinement with respect to their dispersion characteristics, while care should be taken to accurately reproduce the data at the optical limit.
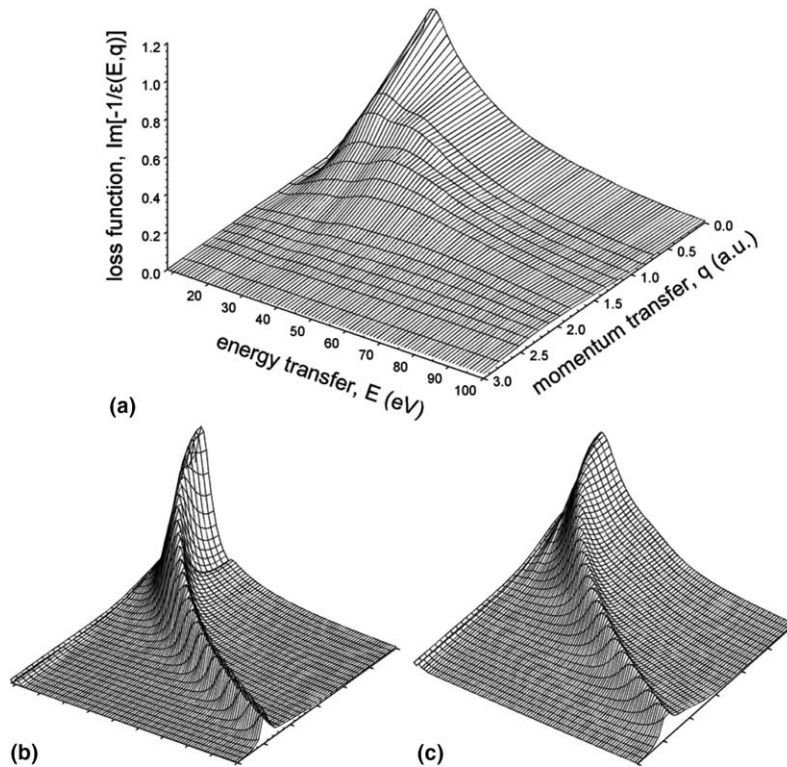
Fig. 3. The Bethe surface of liquid water: (a) experimental IXSS data from [4,5], (b) calculations using the optical-data model established from the reflectance data of [8] and the extended-Drude dispersion, (c) calculations using the optical-data model established from the IXSS data of [4] and the extended-Drude dispersion.
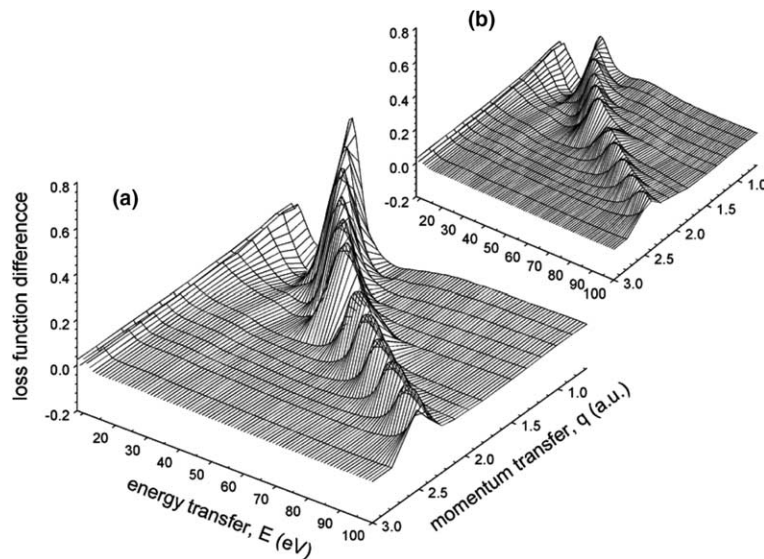
Fig. 4. The difference between the calculated loss function and the experimental loss function obtained from [5]: (a) the model loss function of Fig. 3(b) has been used, (b) the model loss function of Fig. 3(c) has been used.

Acknowledgements

References

[1] U. Fano, Ann. Rev. Nucl. Sci. 13 (1963) 1.
[2] J.M. Fernandez-Varea, Radiat. Phys. Chem. 53 (1998) 235.
[3] D. Emfietzoglou, Radiat. Phys. Chem. 66 (2003) 373.
[4] H. Hayashi, N. Watanabe, Y. Udagawa, C.-C. Kao, Proc. Natl. Acad. Sci. USA 97 (2000) 373.
[5] N. Watanabe, H. Hayashi, Y. Udagawa, Bull. Chem. Soc. Jpn. 70 (1997) 719.
[6] M. Zaider, A.Y.C. Fung, J. Li, J. Ladik, Int. J. Quant. Chem. 80 (2000) 327.
[7] R.H. Ritchie, R.N. Hamm, J.E. Turner, H.A. Wright, J.C. Ashley, G.J. Basbas, Nucl. Tracks Radiat. Measur. 16 (1988) 141.
[8] J.M. Heller, R.N. Hamm, R.D. Birkhoff, L.R. Painter, J. Chem. Phys. 60 (1974) 3483.
[9] D. Emfietzoglou, K. Karava, G. Papamichael, M. Moscovitch, Phys. Med. Biol. 48 (2003) 2355.
[10] D. Emfietzoglou, M. Moscovitch, Nucl. Instr. and Meth. B 193 (2002) 71.
[11] I.G. Kaplan, Nucl. Instr. and Meth. B 105 (1995) 8.
[12] J.M. Fernandez-Varea, R. Mayol, F. Salvat, D. Liljequist, J. Phys.: Condens. Matter 4 (1992) 2879.
[13] A. Akkerman, A. Akkerman, J. Appl. Phys. 86 (1999) 5809.
[14] D. Emfietzoglou, M. Moscovitch, A. Pathak, Nucl. Instr. and Meth. B 212 (2003) 101.
[15] J.C. Ashley, J. Appl. Phys. 69 (1991) 674.
[16] D. Liljequist, J. Phys. D: Appl. Phys. 16 (1983) 1567.
[17] R.H. Ritchie, A. Howie, Philos. Mag. 36 (1977) 463.
[18] ICRU Report 37, Stopping powers for electrons and positrons, Bethesda Maryland, 1984.
[19] H. Bichsel, T. Hiraoka, Nucl. Instr. and Meth. B 66 (1992) 345.
[20] M. Dingfelder, D. Hantke, M. Inokuti, H.G. Paretzke, Radiat. Phys. Chem. 53 (1998) 1.
[21] R.H. Ritchie, R.N. Hamm, J.E. Turner, H.A. Wright, W.E. Bolch, in: W.A. Glass, M.N. Varma (Eds.), Physical and Chemical Mechanisms in Molecular Radiation Biology, Plenum, New York, 1991, p. 99.
[22] W. Friedland, P. Bernhardt, P. Jacob, H.G. Paretzke, M. Dingfelder, Radiat. Prot. Dosim. 99 (2002) 99.
[23] M. Dingfelder, M. Inokuti, Radiat. Environ. Biophys. 38 (1999) 93.